Journal of Materials Chemistry A

PAPER

Cite this: J. Mater. Chem. A, 2017, 5, 17470

Ultrahigh pressure synthesis of highly efficient FeN_x/C electrocatalysts for the oxygen reduction reaction†

Xin Guo,[ab] Xiaopeng Jia,[c] Ping Song,[a] Jing Liu,[ad] Erling Li,[ad] Mingbo Ruan[a] and Weilin Xu *[a]

Received 19th June 2017
Accepted 26th July 2017

DOI: 10.1039/c7ta05334g

rsc.li/materials-a

Ultrahigh pressure (UHP) was employed for the first time as a green method for the synthesis of highly efficient Fe, N co-doped carbon-based (FeN_x/C) electrocatalysts for the oxygen reduction reaction (ORR). Compared with traditional pyrolysis under atmospheric conditions, the synthesis of FeN_x/C catalysts under UHP could be done efficiently with much less consumption of time, energy and chemicals. The observed highly efficient synthesis and high ORR activity of such catalysts could be due to the fast heating system (12 °C per second) under UHP, which leads to highly efficient doping of heteroatoms on carbon with much less consumption of chemicals and energy; the UHP-induced high graphitization degree of the carbon support and the selective formation of highly active sites of pyridinic N and Fe–N_x for the ORR also contribute in part to the high ORR catalytic activity of the catalyst. The work presented here paves a new way for the green, environmentally friendly synthesis of heteroatom-doped highly efficient catalysts for energy or chemical processes.

1. Introduction

With the increasingly severe energy crisis and environmental pollution, fuel cells have attracted extensive interest due to their advantages in sustainable energy conversion, wherein the oxygen reduction reaction (ORR) is a critical process at the cathode of polymer electrolyte fuel cells (PEFCs) for direct conversion of chemical energy into electricity.[1,2] Hence, ORR electrocatalysts with high efficiency are essential for large-scale applications in fuel cells.[3,4] To date, Pt-based materials are known as the most efficient ORR catalysts;[5–7] however, Pt-based materials suffer from many problems in commercial application including prohibitive cost, finite reserves, low durability and CO poisoning effects of Pt.[8,9] Consequently, it is critical to develop energetically highly efficient nonprecious metal catalysts for the ORR to achieve the substitution of Pt-based catalysts. In recent decades, nonprecious metal catalysts, especially, Fe, N co-doped carbon-based catalysts (FeN_x/C) with excellent electrocatalytic performance for the ORR have been well realized to be promising alternative candidates to Pt-based ones.[10,11] However, these catalysts were usually synthesized through pyrolysis at high temperature under atmospheric conditions with a large consumption of chemicals and electricity. Obviously, such an environmentally unfriendly synthesis protocol is time-, energy-, and chemical-consuming. On the other hand, due to the specialty of a sealed ultrahigh pressure (UHP) environment, the UHP technique possesses some unique advantages in preparation and performance improvement of materials. For instance, UHP can effectively modulate phase transformations, morphologies, lattice structures, microstructures, *etc.*, influencing the optical, electrical, and thermal performances of materials.[12,13]

In this work, to deal with the problems in traditional synthesis of heteroatom-doped catalysts, for the first time, the UHP technique was adopted for highly efficient synthesis of FeN_x/C with high ORR electrocatalytic activity.[2,14,15] Such highly efficient synthesis can be done in a short time (down to 5 min) with little consumption of chemicals (such as the nitrogen precursor) and energy (electricity) due to the fast and highly efficient doping of heteroatoms. In this way, the obtained FeN_x/C catalysts with high ORR electrocatalytic activity possess one of the best price/performance ratios and make the method the most environmentally friendly.

2. Experimental procedures

2.1 Materials

Carbon black BP2000 (BP) was purchased from Asian-Pacific Specialty Chemicals Kuala Lumpur. Urea (CH_4N_2O, >99%),

[a]State Key Laboratory of Electroanalytical Chemistry, Jilin Province Key Laboratory of Low Carbon Chemical Power, Changchun Institute of Applied Chemistry, Chinese Academy of Sciences, China. E-mail: weilinxu@ciac.ac.cn

[b]Department of Materials Science and Engineering, Changchun University of Science and Technology, 7989 Weixing Road, Changchun, 130022, P. R. China

[c]State Key Laboratory of Superhard Materials, Jilin University, 2699 Qianjin Street, Changchun, 130012, P. R. China

[d]University of Chinese Academy of Sciences, Beijing, 100049, P. R. China

† Electronic supplementary information (ESI) available. See DOI: 10.1039/c7ta05334g

ferric chloride hexahydrate ($FeCl_3 \cdot 6H_2O$, >99%) and potassium hydroxide (KOH, >85%) were purchased from Sinopharm Chemical Reagent Co. LTD. Nafion solution (5 wt%) was obtained from Sigma-Aldrich. All the chemicals were used as delivered without further treatment. Deionized water with the specific resistance of 18.2 mΩ cm was obtained by reversed osmosis followed by ion-exchange and filtration. The rotating ring-disk electrode of glassy carbon (RRDE, 4 mm in diameter) was purchased from CH Instruments, Inc, USA.

2.2 Preparation of Fe, N co-doped carbon materials

Firstly, the N (urea) and Fe ($FeCl_3 \cdot 6H_2O$) precursors were mixed homogeneously with the carbon support (BP2000 (BP)) by refluxing for 7 hours at 80 °C, as shown in Fig. 1a; secondly, for the UHP experiments (Fig. 1b and S1†), the obtained mixture containing carbon and chemical precursors was pressed tightly to form a φ 10.5 × 2 mm cylinder by cold compression and then was assembled into the sample chamber of a cubic anvil high-pressure apparatus (SPD 6 × 1200), on which a graphite box was used as the heating unit, followed by preparation at 760 °C and under the pressure of 0.85–3.5 GPa for 5 min. The sample chamber was sealed by the UHP exerted from six directions and then heated up rapidly at a rate of 12 °C per second as shown in Fig. 1b. The pressure was calibrated by the change in resistance of standard substances. The synthesis temperature was measured using a Pt RH/Pt Rh6 thermocouple placed near the sample. Finally, the as-prepared catalysts were cracked and ground thoroughly for further electrochemical and physical characterization.

During the pyrolysis in such a sealed chamber, nothing will be leaked out and all the components from the pyrolysis of chemical precursors will be trapped inside. In this way, a tiny amount of precursor can induce highly efficient doping of heteroatoms in short time and then the consumption of chemicals and energy can be reduced hugely, making it a green and environmentally friendly method to replace traditional pyrolysis, in which the gas flow under atmospheric conditions usually leads to a huge consumption or wasting of a large amount of chemicals and energy.

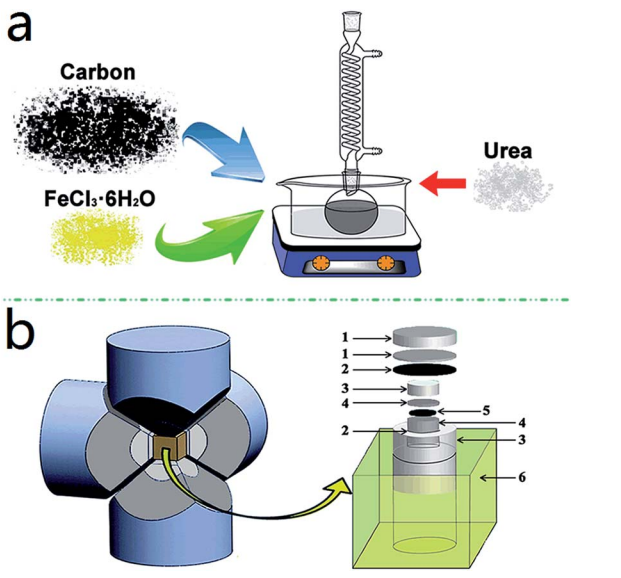

Fig. 1 Scheme of UHP synthesis: (a) precursor processing and (b) UHP synthesis at controllable high temperature and the schematic diagram of the pressure cavity in the cubic anvil high-pressure apparatus, and the assembled chamber ((1)-steel plate, (2)-graphite heater, (3)-dolomitic cylinder, (4)-molybdenum box, (5)-sample, and (6)-pyrophyllite).

2.3 Physical and electrochemical characterization of catalysts

The phase of the as-prepared catalysts was identified by X-ray diffraction (XRD, D/MAX 2500) with Cu-Kα radiation. X-ray photoelectron spectroscopic (XPS) measurements were performed on an AXIS Ultra DLD (Kratos company) using a monochromic Al X-ray source. The microstructures were obtained using a high-resolution transmission electron microscope (HRTEM, JEOL JEM-2100FS). The final N content was determined by elemental analysis (EA) using a vario EL cube (Elementar Analysensysteme Gmbh). The final Fe content was obtained from ICP-MS (ICAP-6000, Thermo Fisher Scientific). The Brunauer–Emmett–Teller (BET) surface areas and pore volumes were obtained from 77 K N_2 sorption isotherms using an ASAP 2020 instrument.

The ORR activity of the as-prepared catalysts was evaluated by voltamperometry on a glassy carbon electrode. Fabrication of the working electrodes was done by pasting catalyst inks on a glassy carbon rotating disk electrode (4 mm in diameter). Its apparent surface area (0.1256 cm^2) was used to normalize the ORR activity of the catalysts. The ink was formed by mixing 5 mg of the catalysts, 50 μL of a 5 wt% Nafion solution in alcohol, and 950 μL of ethanol in a plastic vial under ultra-sonication. A 10 μL ink was dropped on the surface of the glassy carbon rotating disk electrode, yielding an approximate catalyst loading of 0.39 mg cm^{-2}. For comparison, a commercially available platinum/carbon (Pt/C) catalyst, nominally 20 wt% on carbon black from E-TEK was used. The platinum-based ink was obtained by mixing 1 mg catalyst, 50 μL of a 5 wt% Nafion solution in alcohol, and 950 μL of ethanol. Then, a 15 μL platinum ink was dropped on the glassy carbon rotating disk electrode, yielding an approximate loading of 0.015 mg or 24 μg_{Pt} cm^{-2}. The electrolyte was 0.1 M KOH solution; the counter and the reference electrodes were a platinum wire and a SCE electrode (Fig. S2†), respectively. The potential of the electrode was controlled using an EG&G (model 273) potentiostat/galvanostat system. Cyclic voltammetry was performed from 0.2 to −1.2 V at 50 mV s^{-1} after purging the electrolyte with O_2 or N_2 gas for 30 min. Voltamperometry measurements were performed by using a RRDE at a rotating speed of 1600 rpm in an O_2 saturated electrolyte from 0.2 to −1.2 V (*vs.* the SCE) at a sweep rate of 5 mV s^{-1}. The measured potentials *vs.* the SCE were converted to a reversible hydrogen electrode (RHE) scale using the Nernst equation.

For the calculation of H_2O_2 yields of the as-prepared catalysts in 0.1 M KOH, based on both ring and disk currents from the RRDE, the HO_2^-% generated from the ORR and the electron transfer number (n) were estimated by the following equations:

$$HO_2^-\% = 200 \times \frac{i_R/N}{i_D + i_R/N} \quad (1)$$

$$n = 4 \times \frac{i_D}{i_D + i_R/N} \quad (2)$$

where i_D is the disk current density, i_R is the ring current density and N is the current collection efficiency of the Pt ring disk. N is 0.37 from the reduction of $K_3Fe[CN]_6$. All the current densities have already been normalized to the electrode surface area.

3. Results and discussion

To assess the ORR activities of the catalysts obtained under different conditions, linear sweep voltammetry (LSV) tests were performed on a rotating ring disk electrode (RRDE) in O_2-saturated 0.1 M KOH. Based on the half-wave potential ($E_{1/2}$) obtained from LSV curves, the synthesis process was optimized by varying the synthesis temperature (Fig. S3†), time (Fig. S4†), the weight ratio between carbon and urea (Fig. S5†), and pressure (Fig. 2a). The optimal catalyst obtained (under the optimal synthesis conditions: pressure = 1 GPa, pyrolysis temperature = 760 °C, time = 5 min, and mass ratio between BP and urea = 1 : 0.5) finally with Fe 4.7 wt% (ICP-MS) and N 1.67 wt% (elemental analysis) was named BP–NFe. For comparison, the BP, BP–Fe (without urea) and BP–N (without $FeCl_3 \cdot 6H_2O$) were also obtained by UHP method. The traditional pyrolysis method with gas flow under atmospheric conditions was adopted to obtain another FeN_x/C (named P-BP–NFe) at 760 °C for 5 min under atmospheric pressure based on the same amount of raw materials as that for the synthesis of optimal BP–NFe under UHP.

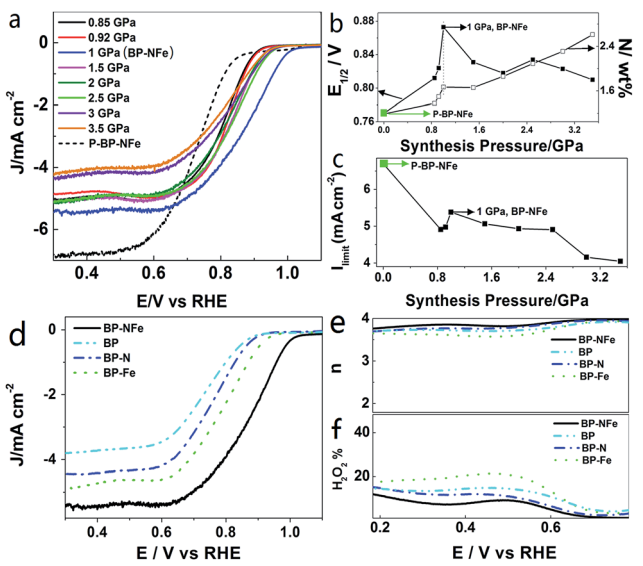

Fig. 2 (a) LSV curves of P-BP–NFe and the FeN_x/C obtained by varying the UHP in O_2 saturated 0.1 M KOH with a scan rate of 5 mV s^{-1} and a rotation speed of 1600 rpm. (b) Synthesis pressure dependences of $E_{1/2}$ and the content of N doped on carbon. (c) Synthesis pressure dependence of the limiting current (I_{limit}). The green points in (b, c) are the values of P-BP–NFe and BP–NFe catalysts. (d) LSV curves of BP, BP–N, BP–Fe and BP–NFe. (e) and (f) are the potential-dependent number of electrons and H_2O_2 yields on these catalysts. The loadings of catalysts are 0.39 mg cm^{-2}.

In particular, as for the pressure-dependence of the ORR performance of catalysts, as shown in Fig. 2b, the half-wave potential ($E_{1/2}$) obtained from LSV curves increases initially with the pressure increase, while after a maximum at 1 GPa, the $E_{1/2}$ decreases inversely with further increase of pressure. The effect of pressure on the ORR performance of the catalysts could also be revealed by the pressure-dependent variation of the diffusion-limiting current as shown in Fig. 2c. Similarly, the limiting current (I_{limit}) increases first with the increase of pressure probably due to the content increase of N doped on carbon, and after a maximum at 1 GPa, the limiting current decreases inversely with pressure although the content of N doped on carbon increases (Fig. 2b). The negative shift of $E_{1/2}$ or the decrease of the limiting current after the maximum probably could be attributed to the compact structure formed at higher pressure, such a compact structure decreases the accessibility of oxygen to the Fe, N-based active sites, and then leads to the decrease of both $E_{1/2}$ and I_{limit} although the total content of N doped on carbon increases continuously with the pressure. Such results indicate that there is an optimal content of N doped on carbon or an optimal pressure in such UHP experiments.[16] Moreover, as shown in Fig. 2a–c, the P-BP–NFe possesses the lowest content of doped N and the lowest $E_{1/2}$ or ORR activity but the largest limiting current. This fact indicates that the number of exposed active sites on P-BP–NFe is much larger than that on UHP-based catalysts although the content of N doped on P-BP–NFe is lower than that on UHP-based catalysts. It further indicates that the intrinsic activity of the exposed active sites on BP–NFe is much higher than those on P-BP–NFe.

The above results indicate that the UHP in an appropriate range can indeed improve the ORR performance of the catalysts, probably due to its significant effect on the doping efficiency of heteroatoms and the microstructure of active sites on carbon. Significantly, as shown in Fig. S6,† the ORR performance of the obtained optimal BP–NFe is even better than that of the commercial Pt/C with Pt 20 wt% indicated by the huge difference of $E_{1/2}$ (0.87 V for BP–NFe *vs.* 0.81 V for Pt/C) and on the same level as other reported best Fe–N-based catalysts (Table S1†) in alkaline.[17–23] As for the advantages of the UHP method over traditional pyrolysis under atmospheric conditions, as shown in Fig. 2, the ORR catalytic activity of optimal BP–NFe is much higher than that of P-BP–NFe, which was obtained with the consumption of the same amount of chemicals but much more energy than that for BP–NFe obtained from UHP.

To deeply understand the high ORR catalytic activity of the optimal BP–NFe, the ORR catalytic activity of BP, BP–Fe (without urea) and BP–N (without Fe) obtained by the UHP method were also studied. As shown in Fig. 2d, the pure carbon BP shows a very low ORR activity. While after the sole doping of N- (BP–N) or Fe- (BP–Fe) on carbon, the ORR activity was improved more or less indicated by the increase of onset potential and limiting current. As expected, after the co-doping of N and Fe on carbon,

the ORR performance on BP–NFe was improved significantly due to the well-known synergistic effect between N and Fe.[24,25] The electron transfer numbers (n) and H_2O_2 yields of these catalysts are also plotted in Fig. 2e and f based on RRDE data. It shows that the H_2O_2 yield on the optimal BP–NFe is the lowest (<10%) among these catalysts in a wide potential range while with the largest n of ~3.9, very close to that of Pt/C ($n \sim 4$). This result indicates that the BP–NFe catalyst in an alkaline medium is a direct four-electron process with water as the main product from the ORR.[26]

To further understand the origin of high ORR activity and the effect of UHP on BP–NFe, the sample was characterized with different techniques. Fig. 3a and b show the typical TEM images of BP–NFe. The iron nanoparticles and the amorphous porous carbon structure with thin-layer graphene-like nanosheets can be seen clearly. Furthermore, from the XRD analysis (Fig. S7†), interestingly, it was found that the iron nanoparticles on BP–NFe mainly exist in the form of Fe_3O_4 nanoparticles (Fig. 3b). The pressure-dependent porous nature of catalysts was further assessed by nitrogen adsorption–desorption analysis as shown in Fig. 3c and d. Fig. 3c shows clearly that the average size of mesopores decreases and the percentage of micropores increases gradually with the pressure increase. Correspondingly, the BET surface area also decreases gradually with the increase of pressure as shown in Fig. 3d. Obviously, the observed decreases of pore size and the BET surface area at higher pressure could be attributed to the UHP-induced formation compact structure. Such a compact structure can prohibit the accessibility of oxygen to the active sites, just like that shown in Fig. 2.

Furthermore, high-resolution XPS was employed to investigate the chemical states of doped N and Fe atoms. As shown in Fig. 4a, the doped N atoms mainly exist in four different bonding states. The peaks at 398.3, 400.1, and 401.1 eV correspond to pyridinic (33.04%), pyrrolic (26.64%) and graphitic (8.82%) N, respectively,[27] while the peak at 399.5 eV is indexed to the Fe–N bond (31.50%).[26] Generally, the active centers based on the Fe–N bond can highly activate the ORR process by the significant decrease of oxygen adsorption energy and extension of the O–O bond.[28–30] Such an observation can explain the observed synergistic effect between doped N and Fe during the ORR process as shown in Fig. 2. In addition, the existence of high contents of pyridinic N also can partially explain the observed high ORR activity since it has been known that pyridinic N is the main active component with the highest ORR activity among different N forms in N-doped metal free catalysts.[24,31] By comparing the N-based chemical states between BP–NFe and P-BP–NFe, as shown in Fig. S8 and Table S2,† it can be seen that the UHP can enhance the formation of highly active sites of Fe–N_x (from 23.58% to 31.50%) and pyridinic N (from 20.75% to 33.04%), confirming the significant role of UHP for the selective formation of highly active sites.

The Fe 2p spectrum of BP–NFe shown in Fig. 4b could be divided into two peaks at 710.4 and 711.3 eV, which can be assigned to the binding energies of the $2p_{3/2}$ orbitals of Fe^{2+} and Fe^{3+} species, confirming the observation of Fe_3O_4 from the HRTEM (Fig. 3b) and XRD (Fig. S7†). Furthermore, from the atomic ratio of $Fe^{3+}/Fe^{2+} = 2$ in Fe_3O_4 and the contents of Fe^{2+} and Fe^{3+} shown in Table S2,† the content of Fe^{2+} in the form of Fe–N_x in the BP–NFe was deduced to be about 6.9%. By comparing it with that (1.0%) on P-BP–NFe as shown in Fig. S8 and Table S2,† one can see that the UHP can enhance the formation of Fe–N_x on the carbon support, consistent with the conclusion made from the N-based component.

Fig. 4c shows the Raman spectra of the P-BP–NFe and BP–NFe catalysts; moreover, Raman spectra of all the catalysts prepared are also summarized in Fig. S9,† including the P-BP–NFe and BP–NFe with the synthesis pressure from 0.85 to 3.5 GPa. It shows clearly that the UHP can lead to the graphitization

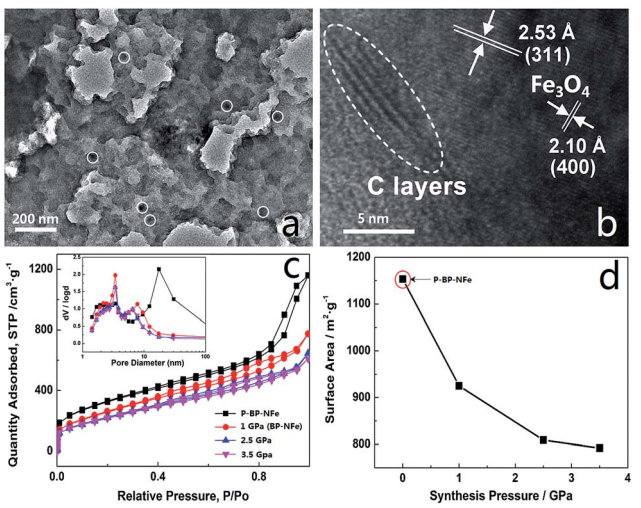

Fig. 3 (a) TEM and (b) HRTEM images of BP–NFe. The white circles indicate the distribution of Fe nanoparticles in (a). (c) Nitrogen adsorption–desorption isotherms, the inset is pore-size distributions; (d) synthesis pressure dependence of the Brunauer–Emmett–Teller (BET) surface area.

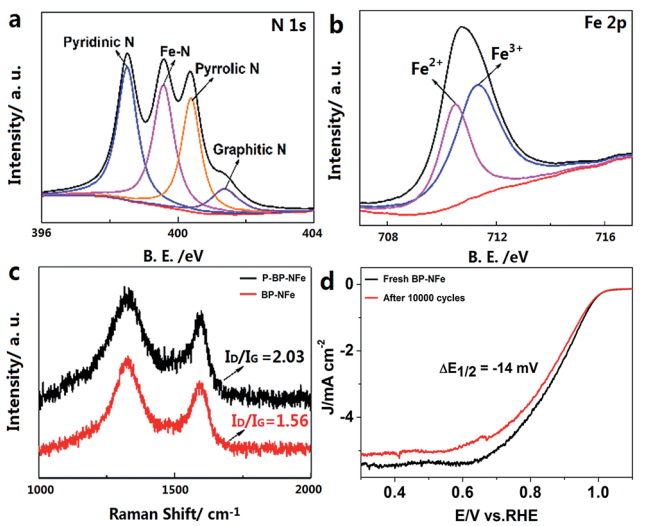

Fig. 4 High-resolution XPS spectra of N 1s (a) and Fe 2p (b) of the BP–NFe catalyst. (c) Raman spectra of the P-BP–NFe and the BP–NFe catalysts. (d) The durability of BP–NFe in O_2-saturated 0.1 M KOH.

of carbon to generate graphene-like nanosheets with the intensity increase of I_G, consistent with the observation from the HRTEM image (Fig. 3b). No significant shifts or line broadening suggests that the carbon structure is mostly retained after the UHP process. It is well known that the carbon graphitization in the catalysts can enhance the electronic conductivity and corrosion resistance in electrocatalysis,[2,32] which then also contribute in part to the observed high ORR performance.

The durability or stability of the optimal catalyst was assessed based on the US Department of Energy's accelerated durability test protocol by cycling the catalyst between 0.6 and 1.15 V at 200 mV s^{-1} in O_2 saturated 0.1 M KOH. As shown in Fig. 4d, the BP–NFe shows a slight decrease of the limiting current and a 14 mV negative shift of $E_{1/2}$ but without a negative shift of the onset potential after 10 000 cycles. The slight decrease of the limiting current probably could be attributed to the loss of catalyst from the electrode surface, while the slight decrease of $E_{1/2}$ represents a deterioration of ORR activity for BP–NFe, which may be ascribed to the collapse of local N- or Fe-based active sites, further impacting the diffusion-limiting current. For comparison, the durability of commercial Pt/C was also tested. As shown in Fig. S10,† due to the migration/aggregation of Pt nanoparticles caused by continuous potential cycling and subsequent loss of the specific catalytic activity, the Pt/C displays a much larger negative shift (24 mV) of $E_{1/2}$ after 5000 cycles. Such a difference thus indicates an excellent long-term operational stability of BP–NFe during the ORR process. As expected, such a catalyst also shows no response to CO and methanol (Fig. S11†).[16,33]

4. Conclusions

In summary, for the first time, ultrahigh pressure (UHP) synthesis was adopted as a green synthesis of highly efficient FeN_x/C electrocatalysts for the ORR with much less consumption of chemicals and energy compared with tradition atmospheric pyrolysis. The obtained optimal catalyst BP–NFe with a remarkable durability shows superhigh ORR performance. It was further found that the UHP can efficiently enhance the doping efficiency of heteroatoms on carbon, the graphitization of carbon, and the selective formation of highly active sites of pyridinic N and Fe–N_x for the ORR. The UHP-based synthesis protocol with much less consumption of chemicals and energy makes the obtained optimal catalyst possess the best performance/price ratio. Such work for the "green" synthesis of highly efficient catalysts opens a new direction for us to explore highly efficient functional materials for energy or industrial processes.

Acknowledgements

This work was supported by the National Basic Research Program of China (973 Program, 2014CB932700), the National Natural Science Foundation of China (U1601211, 21633008, 21433003, 21422307, and 21503212) and the "Recruitment Program of Global Youth Experts" of China. Science and Technology Innovation Foundation of Jilin Province for Talents Cultivation (20160519005JH), China Postdoctoral Science Foundation (2016M601397), Jilin Youth Foundation (20160520137JH), Jilin Science and Technology Development Plan (20170101045JC) and the Open Project of State Key Laboratory of Superhard Materials (Jilin University, No. 201609) are acknowledged.

Notes and references

1 J. Masa, W. Xia, M. Muhler and W. Schuhmann, *Angew. Chem., Int. Ed.*, 2015, **54**, 10102–10120.
2 Q. L. Zhu, W. Xia, T. Akita, R. Q. Zou and Q. Xu, *Adv. Mater.*, 2016, **28**, 6391–6398.
3 M. K. Debe, *Nature*, 2012, **486**, 43–51.
4 G. Wu, K. L. More, C. M. Johnston and P. Zelenay, *Science*, 2011, **332**, 443–447.
5 V. R. Stamenkovic, B. Fowler, B. S. Mun, G. Wang, P. N. Ross, C. A. Lucas and N. M. Marković, *Science*, 2007, **315**, 493–497.
6 C. Wang, H. Daimon and S. Sun, *Nano Lett.*, 2009, **9**, 1493–1496.
7 B. Fang, N. K. Chaudhari, M. S. Kim, J. H. Kim and J. S. Yu, *J. Am. Chem. Soc.*, 2009, **131**, 15330–15338.
8 H. A. Gasteiger, S. S. Kocha, B. Sompalli and F. T. Wagner, *Appl. Catal., B*, 2005, **56**, 9–35.
9 L. M. Dai, *Acc. Chem. Res.*, 2012, **46**, 31–42.
10 X. H. Zhang, P. Lu, X. Z. Cui, L. S. Chen, C. Zhang, M. L. Li, Y. F. Xu and J. L. Shi, *J. Catal.*, 2016, **344**, 455–464.
11 D. Malko, A. Kucernak and T. Lopes, *J. Am. Chem. Soc.*, 2016, **138**, 16056–16068.
12 X. Guo, X. P. Jia, K. K. Jie, H. R. Sun, Y. W. Zhang, B. Sun and H. A. Ma, *CrystEngComm*, 2013, **15**, 7236–7242.
13 J. M. Qin, B. Yao, Y. Yan, J. Y. Zhang, X. P. Jia, Z. Z. Zhang, B. H. Li, C. X. Shan and D. Z. Shen, *Appl. Phys. Lett.*, 2009, **95**, 022101.
14 F. Hu, H. C. Yang, C. H. Wang, Y. J. Zhang, H. Lu and Q. B. Wang, *Small*, 2016, **13**, 1602507.
15 H. T. Wang, S. C. Xu, C. Tsai, Y. Z. Li, C. Liu, J. Zhao, Y. Y. Liu, H. Y. Yuan, F. A. Pedersen, F. B. Prinz, J. K. Nørskov and Y. Cui, *Science*, 2016, **354**, 1031–1036.
16 J. Liu, X. J. Sun, P. Song, Y. W. Zhang, W. Xing and W. L. Xu, *Adv. Mater.*, 2013, **25**, 6879–6883.
17 Y. G. Li, W. Zhou, H. L. Wang, L. M. Xie, Y. Y. Liang, F. Wei, J. C. Idrobo, S. J. Pennycook and H. J. Dai, *Nat. Nanotechnol.*, 2012, **7**, 394–400.
18 J. Y. Cheon, T. Kim, Y. M. Choi, H. Y. Jeong, M. G. Kim, Y. J. Sa, J. Kim, Z. Lee, T. H. Yang, K. Kwon, O. Terasaki, G. G. Park, R. R. Adzic and S. H. Joo, *Sci. Rep.*, 2013, **3**, 2715.
19 N. R. Sahraie, J. P. Paraknowitsch, C. Göbel, A. Thomas and P. Strasser, *J. Am. Chem. Soc.*, 2014, **136**, 14486–14497.
20 P. J. Wei, G. Q. Yu, Y. Naruta and J. G. Liu, *Angew. Chem., Int. Ed.*, 2014, **53**, 6659–6663.
21 N. R. Sahraie, U. I. Kramm, J. Steinberg, Y. J. Zhang, A. Thomas, T. Reier, J. P. Paraknowitsch and P. Strasser, *Nat. Commun.*, 2015, **6**, 8618.
22 Y. J. Sa, D. J. Seo, J. Woo, J. T. Lim, J. Y. Cheon, S. Y. Yang, J. M. Lee, D. Kang, T. J. Shin, H. S. Shin, H. Y. Jeong,

C. S. Kim, M. G. Kim, T. Y. Kim and S. H. Joo, *J. Am. Chem. Soc.*, 2016, **138**, 15046–15056.
23 B. W. Wang, X. X. Wang, J. X. Zou, Y. C. Yan, S. H. Xie, G. Z. Hu, Y. G. Li and A. G. Dong, *Nano Lett.*, 2017, **17**, 2003–2009.
24 W. H. Niu, L. G. Li, X. J. Liu, N. Wang, J. Liu, W. J. Zhou, Z. H. Tang and S. W. Chen, *J. Am. Chem. Soc.*, 2015, **137**, 5555–5562.
25 P. Song, Y. Wang, J. Pan, W. L. Xu and L. Zhuang, *J. Power Sources*, 2015, **300**, 279–284.
26 P. Song, Y. W. Zhang, J. Pan, L. Zhuang and W. L. Xu, *Chem. Commun.*, 2015, **51**, 1972–1975.
27 J. Liu, P. Song and W. L. Xu, *Carbon*, 2017, **115**, 763–772.
28 H. He, Y. Lei, C. Xiao, D. Chu, R. Chen and G. Wang, *J. Phys. Chem. C*, 2012, **116**, 16038–16046.
29 N. Ramaswamy, U. Tylus, Q. Jia and S. Mukerjee, *J. Am. Chem. Soc.*, 2013, **135**, 15443–15449.
30 Y. Zhao, K. Watanabe and K. Hashimoto, *J. Am. Chem. Soc.*, 2012, **134**, 19528–19531.
31 F. L. Meng, Z. L. Wang, H. X. Zhong, J. Wang, J. M. Yan and X. B. Zhang, *Adv. Mater.*, 2016, **28**, 7948–7955.
32 Y. Z. Chen, C. Wang, Z. Y. Wu, Y. Xiong, Q. Xu, S. H. Yu and H. L. Jiang, *Adv. Mater.*, 2015, **27**, 5010–5016.
33 Y. Chen, S. F. Ji, Y. G. Wang, J. C. Dong, W. X. Chen, Z. Li, R. A. Shen, L. R. Zheng, Z. B. Zhuang, D. S. Wang and Y. D. Li, *Angew. Chem., Int. Ed.*, 2017, **56**, 1–6.